Microphone Array Techniques Based on Matrix Inversion

FINEZ Arthur, PICARD Christophe, LE MAGUERESSE Thibaut,
MicrodB, 28 chemin du petit bois, 69131 Ecully Cedex, France

Arthur.finez@microdb.fr

LECLERE Quentin,
Univ Lyon, INSA-Lyon, LVA EA677, F-69621, Villeurbanne, France

PEREIRA Antonio
Ecole Centrale de Lyon – LMFA, 36 Av. Guy de Collongue, 69131 Ecully

ABSTRACT

This lecture series deals with a family of sound source localization techniques based on the solution of minimization problems and make an extensive use of the matrix generalized inverse operator. It is separated from more usual techniques such as beamforming and deconvolution algorithms in the sense that all sources are considered at once (and not separately as in beamforming) and possibly coherent. Basic mathematical principles are presented together with advantages and drawbacks of the technique. Some derivative methods taken from the literature are presented together with application examples in the field of aeroacoustics.

1.0 INTRODUCTION

Microphones array techniques provides a considerable amount of data from which it is possible to extract valuable information on the origin of sound as the location or the power of acoustic sources. The most well spread array method is certainly the beamforming algorithm (also known as “delay-and-sum”) because of its simplicity, robustness and computation efficiency. However it suffers from a lack of resolution in the low frequency range, from the inability to properly quantify the source power, and from the intrinsic hypothesis of uncorrelated and omnidirectional sources which is rarely fulfilled in practical cases. The two first drawbacks have been tackled in the 2000’s with advanced beamforming-based algorithms such as deconvolution techniques. However the uncorrelated source hypothesis remains needed. The beamforming algorithm is indeed essentially a point-to-point method: the estimate of the source strength at each focusing point is sought as if it was the only source in presence. In this context, it is tricky to introduce source correlation in any method which is based on the beamforming principle.

Another family of array methods is considering all the sources at once and is based on matrix inversion; it is the main topic of this lecture series. These methods allow for dealing with correlated, extended or directional sources in a proper formulation, and also offer the possibility to estimate the physical confidence to be accorded to the solution, which is of prime interest for researchers or engineers in experimental techniques.

Inverse techniques are used in the field of vibratory study, a field where the physical phenomena are essentially perfectly coherent, like modal analysis, since a long time [1]. Later, acoustic source analysis (fully and partially coherent sources) based on matrix inversion has first been extensively studied by Nelson and Yoon [2, 3] for general purpose. Nonetheless they can be naturally extended to cases where sources are only partially correlated as in aeroacoustics.

This lectures series is intended to give an introduction course to inverse array methods to researchers or engineers having a background in acoustics but not necessarily in the wide field of inverse techniques

applied to sound source localization and quantification. References in this document are thought to be good entry points for who is willing to dig further a particular aspect. As the number of different array methods is important, it is sometimes difficult to get an overview of their advantages and drawbacks. A didactical comparison of these approaches is presented in reference [4]. It has been chosen here to present a common basis to all these methods in section 2.0 and then to detail some of the most known inverse techniques in section 3.0.

2.0 INVERSE PROBLEM

In this section, the general formulation of the mathematical problem is presented, as well as the standard tools to solve it.

2.1 General underlying formulation

2.1.1 Parameters: measurement data

The first step is to consider a set of measured data at frequency f represented by a column-vector $\boldsymbol{p} \in \mathbb{C}^{\boldsymbol{m}}$ of dimension $[m, 1]$, where m is the number of sensors. $\boldsymbol{p}$ can take many forms, it can be for instance the complex pressure values of a FFT snapshot at frequency f for the microphones in an array, or it can be a more statistically converged input as the principal component of the cross-spectral matrix.

2.1.2 Unknowns: source vector

From this measurement, it is desired to estimate the source amplitude on a grid constituted of n assumed source positions. There is no initial restriction on the source grid, except that it has to be discrete and finite. This means that the grid can be a line, a planar surface, a curved surface or a 3D volume. The sources are represented by a column vector noted $\boldsymbol{q} \in \mathbb{C}^{\boldsymbol{n}}$ of dimension $[n, 1]$. If $\boldsymbol{p}$ is a FFT snapshot, $\boldsymbol{q}$ is expected to be a FFT snapshot of the source amplitudes responsible for the measurement in $\boldsymbol{p}$.

Before going further, it is important to note that an "acoustic source" is usually defined as a minimum region in the physical space for which the acoustic radiated power is not zero. In most aeroacoustic applications it is clear that these sources are continuous and extended volumetric regions, often located in the vicinity of obstacles and turbulent shear region in general. There is no reason for the scanning grid to match perfectly the physical source region. In this regard, it is desired to obtain in $\boldsymbol{q}$ a complex amplitude estimate of *equivalent* sources defined by the scan grid, for which the radiated acoustic power is equal to the radiated power of the physical source region. The meaning of the term "equivalent" is then defined by the propagation model.

2.1.2 Assumed model: transfer matrix

The link between the source and the sensors data is given by a known transfer model which is represented by the complex matrix $\boldsymbol{G}$ of dimension $[m, n]$. Each column of $\boldsymbol{G}$ is thus the equivalent of the steering vector in the beamforming technique. In most cases (but not all), it is chosen as a physical propagation operator: a column of $\boldsymbol{G}$ is the complex pressure generated on all the microphones under the influence of a given unit source located on the scan grid. A common formulation for an element in $\boldsymbol{G}$ is the 3D free field Green function for a microphone i and a source j separated by a distance r_{ij}:

$$\boldsymbol{G}_{ij} = \frac{1}{4\pi}\frac{e^{-\imath k r_{ij}}}{r_{ij}} \tag{0.1}$$

with $k = \frac{2\pi f}{c_0}$ the wavenumber and c_0 the speed of sound and ι the notation for the unit imaginary number to avoid confusion in index i. Analytical expressions of the elements of $\boldsymbol{G}$ can take many forms: it is possible to include reflexion aspects on plane by adding image sources, to include scattering effects or propagation through shear flows using analytical formulations. A numerical software can also be used to compute the propagation function between the source and the microphone including all scattering effects. At last it is possible to directly measure the transfer function using a calibrated small source at the price of a tedious experimental procedure.

2.1.3 Matrix Formulation

The problem of source identification is now reduced to a simple discrete $[m, n]$ linear problem:

$$\boldsymbol{p} = \boldsymbol{G}\boldsymbol{q} \tag{1}$$

Where the unknown vector $\boldsymbol{q}$ is sought given a measured vector $\boldsymbol{p}$ and an assumed propagation matrix $\boldsymbol{G}$. In this expression, $\boldsymbol{p}$ results from the contribution of *all* sources in the scan grid at the same time. This is why this family of method can deal with perfectly correlated sources.

The relation between dimensions m and n determines the nature of the mathematical problem. If there are less microphones than assumed source position ($m < n$), there are more unknowns than independent equations. The problem is said under-determined and there exist an infinity of distinct solutions satisfying equation (1). On the contrary if $m > n$, there are more independent equations than unknowns, the problem is over-determined and it is most certain that there exists no vector $\boldsymbol{q}$ solving exactly equation (1).

In practice, the number of equivalent sources used for representing the source is usually higher than the number of available measurements. This leads to an under-determined and ill-posed problem in the sense of Hadamard[1]: it has an infinite number of solutions. A choice has to be made among all these solutions; it should be based on an additional criterion which is defined in the following.

2.2 Pseudo-inverse solution for underdetermined systems

2.2.1 General properties

A powerful tool for solving equation (1) is the Moore-Penrose pseudo-inverse operator. It is a generalization of the matrix inverse operator and valid for non-squared matrix. The pseudo inverse matrix of $\boldsymbol{G}$ noted $\boldsymbol{G}^+$ is the only matrix $[n, m]$ satisfying the following three conditions

$$\boldsymbol{G}\boldsymbol{G}^+\boldsymbol{G} = \boldsymbol{G} \tag{2.1}$$

$$\boldsymbol{G}^+\boldsymbol{G}\boldsymbol{G}^+ = \boldsymbol{G}^+ \tag{2.2}$$

$\boldsymbol{G}\boldsymbol{G}^+$ and $\boldsymbol{G}^+\boldsymbol{G}$ are Hermitian matrices (2.3)

It is a less restrictive version of the conditions required for the standard inverse $\boldsymbol{A}^{-1}$of a squared matrix $\boldsymbol{A}$: $\boldsymbol{A}^{-1}\boldsymbol{A} = \boldsymbol{A}\boldsymbol{A}^{-1} = \boldsymbol{I}$. Besides in the specific case of full-rank squared matrices, $\boldsymbol{A}^+$ is equal to the standard inverse matrix $\boldsymbol{A}^{-1}$ [5].

Assuming that such a matrix is available, it is clear that a source vector built on $\boldsymbol{G}^+$using $\tilde{\boldsymbol{q}} = \boldsymbol{G}^+\boldsymbol{p}$ is a solution of (1) since $\boldsymbol{G}\tilde{\boldsymbol{q}} = \boldsymbol{G}\boldsymbol{G}^+\boldsymbol{p} = \boldsymbol{G}\boldsymbol{G}^+\boldsymbol{G}\boldsymbol{q} = \boldsymbol{G}\boldsymbol{q} = \boldsymbol{p}$. The pseudo-inverse is thus a tool to provide one of the exact solutions of problem (1). This specific solution has an additional interesting property: it can be demonstrated that solution $\tilde{\boldsymbol{q}}$ is the exact solution of (1) with the smallest 2-norm:

[1] The three conditions for a well-posed problem suggested by Hadamard are existence, uniqueness, stability of the solution.

$$\tilde{\boldsymbol{q}} = \boldsymbol{G}^{+}\boldsymbol{p} \;= \underset{\boldsymbol{q}\in\mathbb{C}_n}{\operatorname{argmin}}(\|\boldsymbol{q}\|_2 \text{ such that } \boldsymbol{p} = \boldsymbol{G}\boldsymbol{q}) \tag{3}$$

Actually this minimum 2-norm property is one possible aforementioned selection condition among all solutions of (1). It can be physically justified because $\|\tilde{\boldsymbol{q}}\|_2$ can be seen as the total energy of the source region solution and the minimization of this quantity can be linked to the general principle of least action.

2.2.2 Practical calculation

An algorithm[2] to compute $\boldsymbol{G}^{+}$ is based on the Singular Value Decomposition (SVD) of matrix $\boldsymbol{G}$. As the pseudo-inverse is a generalization of the inverse operator, the SVD is a generalization of the Eigen Value Decomposition for non-squared matrices. Any rectangular matrix $\boldsymbol{G}$ of size $[m,n]$ can be decomposed in a unique way into three matrices such that

$$\boldsymbol{G} = \boldsymbol{U}\boldsymbol{S}\boldsymbol{V}^{*} \tag{4}$$

$\boldsymbol{U}$ being a unitary matrix of size $[m,m]$ such that $\boldsymbol{U}\boldsymbol{U}^{*} = \boldsymbol{U}^{*}\boldsymbol{U} = \boldsymbol{I}_{mm}$, $\boldsymbol{V}$ is a unitary matrix of size $[n,n]$ such that $\boldsymbol{V}\boldsymbol{V}^{*} = \boldsymbol{V}^{*}\boldsymbol{V} = \boldsymbol{I}_{nn}$. $\boldsymbol{V}^{*}$ stands for the conjugate transpose (hermitian) matrix of $\boldsymbol{V}$. The $\boldsymbol{S}$ matrix is a rectangular diagonal $[m,n]$ matrix (i.e. such that $\boldsymbol{S}_{ij} = 0$ if $i \neq j$). The diagonal elements of $\boldsymbol{S}$ are called "singular values" (SV); they are all positive and sorted in decreasing order. Based on $\boldsymbol{S}$, another diagonal matrix $\boldsymbol{S}^{+}$ of size $[n,m]$ can be calculated following:

$$\boldsymbol{S}^{+}_{ii} = \frac{1}{\boldsymbol{S}_{ii}} \text{ if } \boldsymbol{S}_{ii} \neq 0 \tag{5}$$

$$\text{else } \boldsymbol{S}^{+}_{ij} = 0, \forall i \leq n, j \leq m$$

The matrix $\boldsymbol{S}^{+}$is actually the pseudo-inverse of matrix $\boldsymbol{S}$ because it satisfies conditions (2). The pseudo-inverse of $\boldsymbol{G}$ can then be constructed using $\boldsymbol{S}^{+}$following $\boldsymbol{G}^{+} = \boldsymbol{V}\boldsymbol{S}^{+}\boldsymbol{U}^{*}$. It can be checked easily that $\boldsymbol{V}\boldsymbol{S}^{+}\boldsymbol{U}^{*}$ also satisfies conditions (2). As a summary, the solution $\tilde{\boldsymbol{q}} = \boldsymbol{G}^{+}\boldsymbol{p}$ is the exact solution of problem (2) with the smallest 2-norm. This formula generates satisfying results in the case of a simulated monopole without additional noise for instance.

2.2.3 Stability analysis

However the naive pseudo-inverse solution suffers from a major drawback: the solution $\tilde{\boldsymbol{q}}$ may not be stable under small variations in either $\boldsymbol{p}$ or $\boldsymbol{G}$. The ability of the problem to produce stable or unstable solutions is called its conditioning; it is quantified by the condition number

$$\sigma = \|\boldsymbol{G}\|_F \|\boldsymbol{G}^{+}\|_F \tag{6}$$

Where$\|\boldsymbol{G}\|_F = \sqrt{\sum_{i=1}^{m}\sum_{j=1}^{n}|\boldsymbol{G}_{ij}|^2}$ is the Frobenius norm of matrix $\boldsymbol{G}$. The link between σ and the stability characteristics is the following: considering a small variation $\boldsymbol{\delta p}$ in the measured vector, a variation in the estimated solution $\boldsymbol{\delta\tilde{q}}$ is induced. Since problem (1) is linear, we have the relationship $\boldsymbol{\delta\tilde{q}} = \boldsymbol{G}^{+}\boldsymbol{\delta p}$, which implies the norm inequality $\|\boldsymbol{\delta\tilde{q}}\|_2 \leq \|\boldsymbol{G}^{+}\|_F \|\boldsymbol{\delta p}\|_2$. At the same time, since $\boldsymbol{p} = \boldsymbol{G}\tilde{\boldsymbol{q}}$, we have $\|\boldsymbol{p}\|_2 \leq \|\boldsymbol{G}\|_F \|\tilde{\boldsymbol{q}}\|_2$. Combining these two inequalities leads to

$$\frac{\|\boldsymbol{\delta\tilde{q}}\|_2}{\|\tilde{\boldsymbol{q}}\|_2} \leq \|\boldsymbol{G}^{+}\|_F \|\boldsymbol{G}\|_F \frac{\|\boldsymbol{\delta p}\|_2}{\|\boldsymbol{p}\|_2} = \sigma \frac{\|\boldsymbol{\delta p}\|_2}{\|\boldsymbol{p}\|_2} \tag{7}$$

[2] The SVD algorithm to compute the pseudo-inverse matrix is interesting because of the possibility to easily compute a regularized solution as will be presented in section 2.3.2

In other words, the relative variation of the norm of the solution under variations of the measurement is bounded by the condition number σ which depends only on the model matrix $\boldsymbol{G}$. This explains its crucial role in the sensitivity analysis of the problem.

A different view angle can explain the role of σ. It can be demonstrated that an equivalent mathematical expression for σ is

$$\sigma = \frac{\boldsymbol{S}_1}{\boldsymbol{S}_m} \tag{8}$$

Where S_1 is the highest singular value of G and $S_m$is the minimal singular value. The latter represents the smallest contribution to $\boldsymbol{p}$ in the direct problem $\boldsymbol{p} = \boldsymbol{Gq}$ but leads to the highest contribution in the estimated solution $\tilde{\boldsymbol{q}}$ (because $\boldsymbol{S}_m^+ = 1/\boldsymbol{S}_m$). On the contrary $\boldsymbol{S}_1$ is the maximal singular value of $\boldsymbol{G}$; it represent the most significant contribution to $\boldsymbol{p}$ in the direct problem but leads to the smallest component in $\tilde{\boldsymbol{q}}$. Considering that we deal with measured data $\boldsymbol{p}$, those minor contributions in the direct problem are often tarnished with noise, which should not be unreasonably amplified in the inversion procedure. In practice, this leads to solutions for which small deviations on the measured data are matched at the price of very large fluctuations of the source vector. The obtained result is most probably highly different from the physical solution. The sensitivity to measurement noise can then be estimated by the ratio of the highest SV to the smallest non-zero SV. This matches expression (8) given for the condition number σ.

The condition number is by construction higher than 1 and is an indicator of how difficult problem (1) will be to solve. The closer to 1 σ is, the less sensitive to noise matrix $\boldsymbol{G}$ will be. Typical values above which the inversion becomes really difficult is 10^3. Since σ depends only on matrix $\boldsymbol{G}$, no measurement is needed in this analysis. The minimization of σ can be a powerful tool to optimize the array microphone locations.

2.3 Regularization

In the last section we have seen that the naive pseudo-inverse operator leads in underdetermined conditions to an exact solution of the problem $\boldsymbol{p} = \boldsymbol{Gq}$, the one which has the minimum 2-norm. In practice, this solution can be subject to instability which is due to the inversion of smallest singular values in the model matrix. The principle of controlling the irregularity of the inverse problem has produced a furnished literature on "regularization procedures". Only a reduced number is presented in this document.

2.3.1 TSVD

A first pragmatic approach is to get rid of those undesired "small" singular values. Assuming that we have determined a minimum SV $\boldsymbol{S}_{m_0}$ to consider, we can compute a degraded matrix $\boldsymbol{S}^{(m_0)+}$ which only accounts for the SV above this threshold,

$$\boldsymbol{S}_i^{(m_0)+} = \frac{1}{\boldsymbol{S}_{ii}} \text{ if } \boldsymbol{i} \leq m_0 \tag{9}$$

$$\text{else } \boldsymbol{S}_{ij}^{(m_0)+} = 0$$

A degraded pseudo-inverse $\boldsymbol{G}^{(m_0)+} = \boldsymbol{V}\boldsymbol{S}^{(m_0)+}\boldsymbol{U}^*$is then used. This type of regularization is called "Truncated Singular Value Decomposition". High amplitude fluctuations in $\tilde{\boldsymbol{q}}$ are indeed reduced but the solution may not be convergent in m_0, in the sense that neighbour values for m_0 give rise to very different results. It is then difficult to choose the closest one to the physical solution.

2.3.2 Tikhonov regularization

Another approach is to apply a smooth filter on the singular values using a real quantity λ called the regularization parameter. The idea is to attenuate the influence of smallest SV while leaving almost unchanged the highest ones, with a progressive transition. This approach is known as the "Tikhonov regularization" or "ridge regression" in the field of statistics. The practical expression used for the S inversion reads

$$\boldsymbol{S}_i^{(\lambda)+} = \frac{\boldsymbol{S}_{ii}}{\boldsymbol{S}_{ii}^{\boldsymbol{2}}+\lambda^{\boldsymbol{2}}} \tag{10}$$

If λ is correctly chosen, for highest singular values $\boldsymbol{S}_{ii}^{\boldsymbol{2}} \gg \lambda^{\boldsymbol{2}}$ and $\boldsymbol{S}_i^{(\lambda)+} \cong \frac{1}{\boldsymbol{S}_{ii}}$ which is the expected result. For the smallest one $\boldsymbol{S}_{ii}^{\boldsymbol{2}} \ll \lambda^{\boldsymbol{2}}$ and $\boldsymbol{S}_i^{(\lambda)+} \cong \frac{\boldsymbol{S}_{ii}}{\lambda^{\boldsymbol{2}}}$. Now the contribution to $\boldsymbol{S}^{(\lambda)+}$ of the smallest SV are all the more mitigated than they are small, which answers to the instability problem. After regularization, the effective condition number is greatly reduced:

$$\sigma^{(\lambda)} = \frac{\boldsymbol{S}_m^{(\lambda)+}}{\boldsymbol{S}_1^{(\lambda)+}} \cong \frac{\boldsymbol{S}_m \boldsymbol{S}_1}{\lambda^{\boldsymbol{2}}} \ll \frac{\boldsymbol{S}_1}{\boldsymbol{S}_m} = \sigma \tag{11}$$

To work properly, the regularization parameter should be carefully selected since its value may lie in the range $[\boldsymbol{S}_m, \boldsymbol{S}_1]$ in unstable cases. The highest this parameter, the stronger the regularization. Moreover in stable cases, when σ is close to 1, the regularization parameter should be close to 0, since formulation (6) is entirely satisfying. Procedures for automatic selection of the Tikhonov regularization parameter are also numerous, some are presented in section 2.4.3.

It is interesting to note that the regularized solution $\tilde{\boldsymbol{q}}^{(\lambda)} = \boldsymbol{V}\boldsymbol{S}^{(\lambda)+}\boldsymbol{U}^{*}\,\boldsymbol{p}$ is not a solution of (1): the residue $\left\|\boldsymbol{p} - \boldsymbol{G}\tilde{\boldsymbol{q}}^{(\lambda)}\right\|_{\boldsymbol{2}}$ is not zero because $\boldsymbol{S}\boldsymbol{S}^{(\lambda)+} \neq \boldsymbol{I}_{\boldsymbol{mm}}$. While the initial problem can be formulated as the minimization of the cost function $\|\boldsymbol{p} - \boldsymbol{G}\boldsymbol{q}\|_{\boldsymbol{2}}$, $\tilde{\boldsymbol{q}}^{(\lambda)}$ is the solution of another least square problem, called the Tikhonov problem:

$$\tilde{\boldsymbol{q}}^{(\lambda)} = \operatorname{argmin}_{\boldsymbol{q}\in\mathbb{C}^{\boldsymbol{n}}}\{\|\boldsymbol{p} - \boldsymbol{G}\boldsymbol{q}\|_2^2 + \lambda^2\|\boldsymbol{q}\|_2^2\} \tag{12}$$

Expression (12) can be interpreted as the fact that the amplitude of the solution $\left\|\tilde{\boldsymbol{q}}^{(\lambda)}\right\|_{\boldsymbol{2}}$ is controlled at the price of a small increase in the fit error $\left\|\boldsymbol{p} - \boldsymbol{G}\tilde{\boldsymbol{q}}^{(\lambda)}\right\|_{\boldsymbol{2}}$. The balance is set by the parameter λ. In other words, we have introduced the *a priori* information that the 2-norm of the source should not be too large, which allowed us to slightly modify the initial problem and find a solution which is more likely to be close to the physical situation than the naïve solution. Equalling $\|\boldsymbol{p} - \boldsymbol{G}\boldsymbol{q}\|_{\boldsymbol{2}}$ to 0 and finding the solution with the minimum $\|\boldsymbol{q}\|_{\boldsymbol{2}}$ is not equivalent to jointly minimize $\|\boldsymbol{p} - \boldsymbol{G}\boldsymbol{q}\|_{\boldsymbol{2}}$ and $\|\boldsymbol{q}\|_{\boldsymbol{2}}$.

2.3.3 Regularization parameter selection

In the Tikhonov regularization procedure, the choice of the parameter λ plays a crucial role. Several selection strategies can be mentioned. In this document, we are presenting the most common one, the L-curve technique.

The L-curve is one of the standard tool to select an appropriate value for λ. The idea is to note that noisy data are more likely to stimulate the instability of the inversion. They require a stronger regularization than clean data. Consequently, the chosen value for λ should depend on $\boldsymbol{p}$. A wide range of parameter is tested and the solution $\tilde{\boldsymbol{q}}^{(\lambda)} = \boldsymbol{G}^{(\lambda)+}\boldsymbol{p}$ is computed for each value of λ. Both the residual norm $\left\|\boldsymbol{p} - \boldsymbol{G}\tilde{\boldsymbol{q}}^{(\lambda)}\right\|_{\boldsymbol{2}}$

and the solution norm $\left\|\tilde{\boldsymbol{q}}^{(\lambda)}\right\|_2$ are plotted against each other in log scales. It is expected that this plot (called 'L-curve plot') exhibits a favourable trade-off between these two quantities. An example of this plot is proposed in Figure 1 for a microphone array configuration depicted in the legend. The condition number of $\boldsymbol{G}$ in this case is $1.3 * 10^9$, which indicates that the problem is highly unstable. For array techniques such situations typically arise in the low frequency range because the steering vector between two scan points are almost collinear.

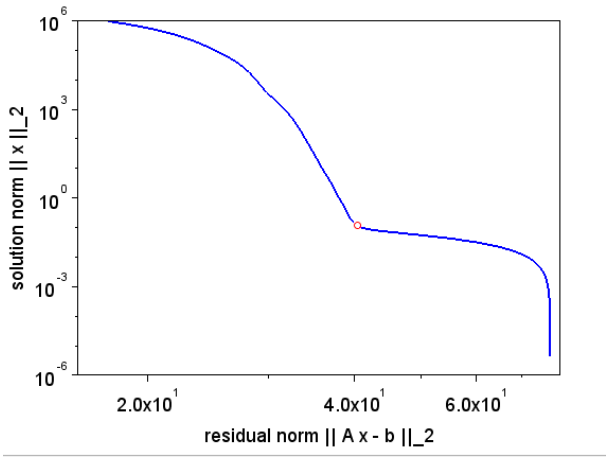

Figure 1: L-curve for the simulated case of a monopole in free field, situated in front of an array of 54 microphones, 50cm diameter and situated 50cm away from the array. F=50 Hz, the square grid is twice the width of the array, SNR = 0 dB.

Solutions in the top-left corner of Figure 1 correspond to low values of λ: the regularization is too weak, the residue is close to zero but the solution norm is very high. In opposition, in the bottom-right corner, high values of λ represent over-regularized solutions for which the system is highly damped: the residue is very high and the solution norm is close to zero. In many cases, the obtained curve forms a L-shape, it is convex and a particular point can be located at the bottom of the elbow, represented by a red circle on Figure 1. This point corresponds to the optimized value of λ rendered by the L-curve method. Departing from this point will either produce a high increase in the solution amplitude or in the fit error.

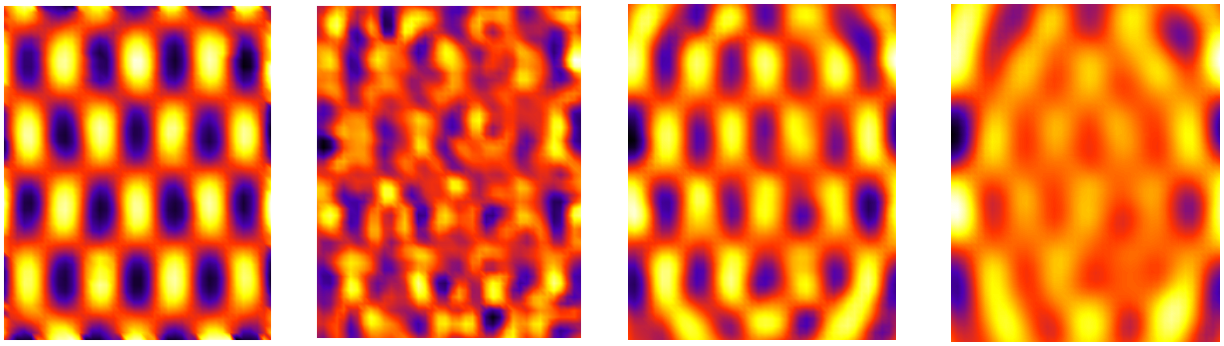

(a) Reference (b) $\frac{\lambda_{\text{opt}}}{10}$, C = 45% (c) λ_{opt}, C = 60% (d) $10\lambda_{\text{opt}}$, C = 28%

Figure 2: Pressure map of a vibrating plate at 397 Hz reconstructed using various values of the regularization parameter λ, from [8]. (a) Reference pressure field, (b) solution using a low value $\lambda = \lambda_{\text{opt}}/10$, (c) solution using an optimal value $\lambda = \lambda_{\text{opt}}$, (d) solution using a high value $\lambda = 10\lambda_{\text{opt}}$. The same color bar has been used for the four plots.

An illustration of these situations is given in Figure 2. It is extracted from examples given in the didactical paper by [8]. A vibrating plate is simulated and radiated pressure signals are generated at the microphone locations with the addition of noise. An inverse technique (Near-field acoustic holography) is used to estimate the pressure field on the plate surface from these synthetic data. Figure 2.a is the reference pressure field which is analytically computed, Figure 2.b is the reconstruction pressure field using an under-regularized inverse process. The characteristic length of pressure fluctuations on the plate is much smaller than on the reference case. The modal pattern can hardly be recognized. The match between the reference field and the reconstructed field can be evaluated by the covariance coefficient C indicated below the figures. Figure 2.c is constructed using an optimized value of the regularization parameter. The initial pattern is almost perfectly recovered. Figure 2.d is constructed with a higher value of λ. The massive damping of the solution is clearly visible.

2.3.4 Alternative regularization

The choice of minimal $\left\|\tilde{\boldsymbol{q}}^{(\lambda)}\right\|_2$ as the *a priori* information to control the solution in eq. (12) seems natural but somewhat arbitrary. It is absolutely possible to introduce other controls, as to use a matrix $\boldsymbol{C}$ as in the following problem

$$\text{minimize}: \ \|\boldsymbol{p} - \boldsymbol{G}\boldsymbol{q}\|_2^2 + \lambda^2\|\boldsymbol{C}\boldsymbol{q}\|_2^2 \tag{13}$$

If $\boldsymbol{C}$ is correctly chosen, it can be used to control the smoothness of the solution via the discrete derivative coefficients. This leads to the family of methods related to Iterative Reweighted Least Squares (IRLS).

Another idea is to impose the number of non-zero elements in the source map $\|\boldsymbol{q}\|_0 = \text{card}\{\boldsymbol{q_i} \,/\, |\boldsymbol{q_i}| \neq \boldsymbol{0}\}$ to be as small as possible. It is assumed that the number of true sources is in small number or located in a very small region of the source map. This is a way to control the sparsity of the solution and it leads to the new problem:

$$\text{minimize}: \ \|\boldsymbol{p} - \boldsymbol{G}\boldsymbol{q}\|_2^2 + \lambda^2\|\boldsymbol{q}\|_0 \tag{14}$$

Unfortunately this problem happens to be very difficult to solve since it is known to be a non-convex mathematical problem. Instead, it is chosen to try a relaxed form of problem (14) using the L1 norm $\|\boldsymbol{q}\|_1 = \sum_{i=1}^{n}|\boldsymbol{q_i}|$ raising the Lasso problem

$$\text{minimize}: \ \|\boldsymbol{p} - \boldsymbol{G}\boldsymbol{q}\|_2^2 + \lambda^2\|\boldsymbol{q}\|_1 \tag{15}$$

This last problem is the starting point of a lot of identification methods based on source sparsity assumption [6-10].

Two methods belonging to the IRLS family and associated with Lp-norm (with $0 \leq p \leq 2$) will be discussed later (§3.4).

3.0 APPLICATION METHODS

The general inverse approach detailed in section 2.0 has been developed in various versions to address the practical problem of sound source localization and quantification. Each of them has a different understanding of the measured vector $\boldsymbol{p}$ or the unknown source vector $\boldsymbol{q}$. A major difference between them also resides in the displayed quantities. These particularities make the methods suited for some situations and not for others.

Some of them are presented in this section: the acoustical holography, the iBEM method, the inverse Equivalent Source Method, the Generalized inverse beamforming, the Bayesian Inference; we will try to underline their special features.

3.1 Plane wave acoustical holography

3.1.1 Standard acoustical holography

The acoustical holography (AH) technique appeared in the 1960's. It aims at reconstructing the planar pressure[3] field on a source plane from a set of distant microphone measurements on another plane. Since the geometry is planar, it appears natural to work with plane wave components of the sound field, so as to formulate the problem in the wavenumber domain. Plane waves are described as functions of physical coordinates (x, y) while the propagation is described along z. The source plane is located at $z = z_s$ while the measurement plane is at $z = z_h$ In this technique, $\boldsymbol{p}$ is composed of wavenumber Fourier components of the measured pressure sound field at a given frequency $p(x, y, z_h, \omega)$:

$$\boldsymbol{p} = \boldsymbol{\mathcal{F}_x}\boldsymbol{\mathcal{F}_y}(p(x, y, z_h, \omega)) \tag{16}$$

Where $\boldsymbol{\mathcal{F}_x}$ stands for the Discrete Fourier Transform in the x-direction according to the available arrangement of sensors. The dimension m of $\boldsymbol{p}$ is subject to the sampling criterion and is limited by the extent of the array and the spacing between microphones.

Similarly the source vector $\boldsymbol{q}$ is constituted of the wavenumber Fourier components of the pressure sound field on the reconstruction plane at $z = z_s$:

$$\boldsymbol{q} = \boldsymbol{\mathcal{F}_x}\boldsymbol{\mathcal{F}_y}(p(x, y, z_s, \omega)) \tag{17}$$

The elements of the matrix $\boldsymbol{G}$ are the transfer function from the reconstruction plane $z = z_s$ to the measurement plane $z = z_h$. The i-th element in $\boldsymbol{q}$ and $\boldsymbol{p}$ are both plane wave components of axial wavenumber $k_z^{(i)} = \sqrt{k^2 - k_x^{(i)2} - k_y^{(i)2}}$; thus $\boldsymbol{G}_{ij}$simply reduces to :

$$\boldsymbol{G}_{ij} = e^{\iota k_z^{(i)}(z_h - z_s)} \text{ if } i = j \tag{18}$$

$$\boldsymbol{G}_{ij} = 0 \text{ if } i \neq j$$

One can see that the transfer matrix is diagonal, which makes the formal resolution of (1) a trivial task. An additional restriction is made ; only the propagative plane waves are considered, those for which $k_z^{(i)}$ is real. In this case, the problem is well-posed and the existence and the uniqueness of the solution is guaranteed. Moreover the inverse matrix is easily computed since it is also a diagonal matrix: $\boldsymbol{G_{ii}^{-1}} = e^{-\iota k_z^{(i)}(z_h - z_s)}$. This allows to estimate $\tilde{\boldsymbol{q}} = \boldsymbol{G^{-1}p}$. The pressure field on the source plane is finally computed using the double spatial inverse Fourier transform of $\tilde{\boldsymbol{q}}$:

$$\tilde{\boldsymbol{p}}(x, y, z_s, \omega) = \boldsymbol{\mathcal{F}_x^{-1}}\boldsymbol{\mathcal{F}_y^{-1}}(\tilde{\boldsymbol{q}}) \tag{19}$$

The results are displayed as a pressure map in the reconstruction plane which is a bit specific to this method since inverse method often directly plot the source amplitude $\tilde{\boldsymbol{q}}$ in dB.

[3] Or the three components of the surface velocity field, or the acoustic intensity vector

3.1.2 Nearfield Acoustical Holography

In the standard AH, the spatial resolution is limited to half the acoustic wavelength since the source plane is described using propagative plane waves. This is a real limitation, especially at low frequencies. To overcome this drawback, Nearfield Acoustical Holography (NAH) was developed in the 1980s [11-14] and revolutionized the field of diagnosis of acoustic radiation of vibrating structures. The idea is to include a limited number of evanescent waves in the model matrix $\boldsymbol{G}$. In other words, terms of the DFT of $p(x, y, z_h, \omega)$ for which $k^2 < k_x^{(i)2} + k_y^{(i)2}$ are not dumped anymore. Provided that the array is located in the near-field of the source plane, the higher wavenumber components add spatial information to the solution. The resolution is far better than in the standard AH. The counter-effect is that $k_z^{(i)} = ik_z^{(i)\prime}$ is now a pure imaginary number and the inversion formula becomes $\boldsymbol{G}_{ii}^{-1} = e^{k_z^{(i)\prime}(z_h - z_s)}$: evanescent waves are exponentially increased during the back-propagation process and the higher the axial wave number $k_z^{(i)\prime}$ the higher this exponential amplification. The stability problem arises again. As a consequence a regularization procedure is undertaken which is very similar to the Tikhonov technique: the smallest components in $\boldsymbol{G}$ are damped, those corresponding to the highest wavenumbers. A cut-off frequency for the k-space filter is then chosen in a specific way depending on the measurement and the offset $z_h - z_s$ among others. The cut-off frequency is thus a regularization parameter with the physical meaning of a spatial low-pass filter.

3·1·2·1 First laboratory experiment

A laboratory example is given as the first historical application of NAH by [13]. They used an innovative and powerful measurement system (in 1985) with 256 microphones (**Figure 3** left) to image two airborne sound sources. The array is placed in the extreme near field of the sources in order to measure the evanescent wave components. Consequently source directivity and total power radiated into the half-space above the source can properly be estimated.

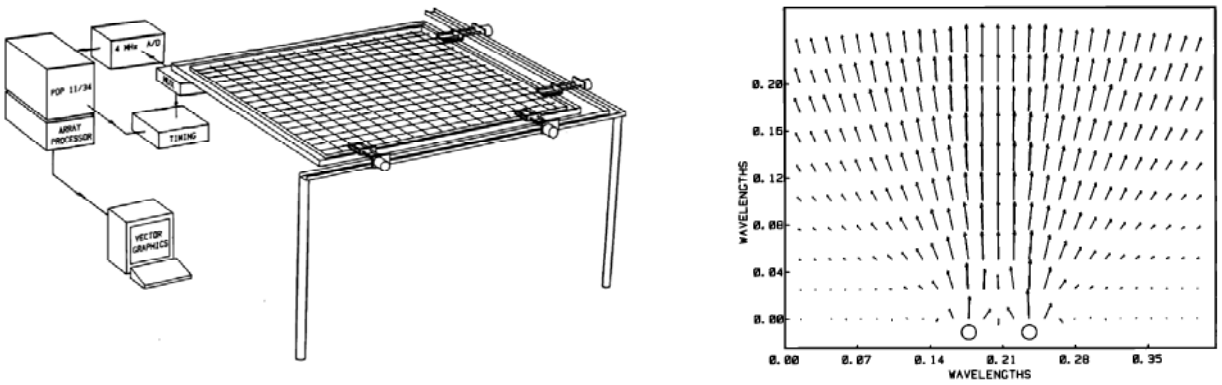

Figure 3: (left) Sketch of the measurement system used by [13] for Nearfield acoustical holography, (right) Computed acoustic intensity vector field from two point source

A 64 x 64 point hologram is calculated with standard holography and NAH. The comparison in **Figure 4** exhibits the advantage of taking into account evanescent plane waves. Acoustic vector intensity field (energy flow patterns) is also calculated in a plane containing the two point sources and perpendicular to the hologram plane (**Figure 3** right).

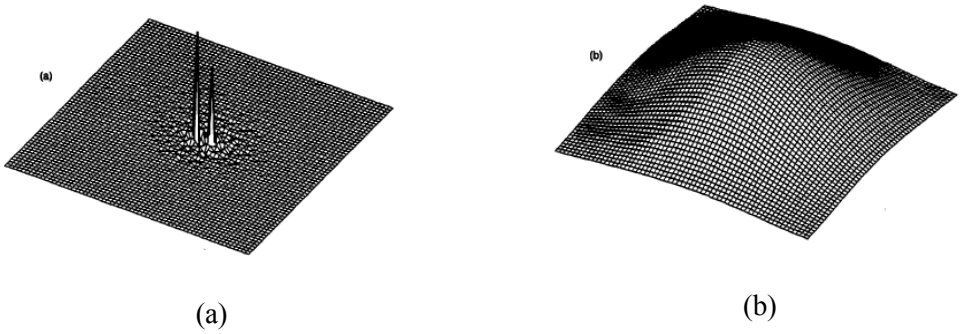

Figure 4: Holographic reconstruction of the intensity of two point sources (a) Nearfield Holography (b) conventional Holography. From [13].

3·1·2·2 Wind tunnel experiment

NAH has also been applied to wind tunnel experiments. Hald & al.[15] used a moving microphone array on the side of a car in the Honda low-noise wind tunnel with a flow speed of 100 km/h. The scanned plane is defined at a distance of 250 mm from the center of the side window. A reference microphone installed in the vehicle is used to synchronize the different array location measurements; this allows to reject microphone self-noise and wind tunnel back ground noise. It is then possible to make holographic calculations [16] for precise localization of the turbulence noise sources and provide valuable information in car noise comparison in the low frequency range.

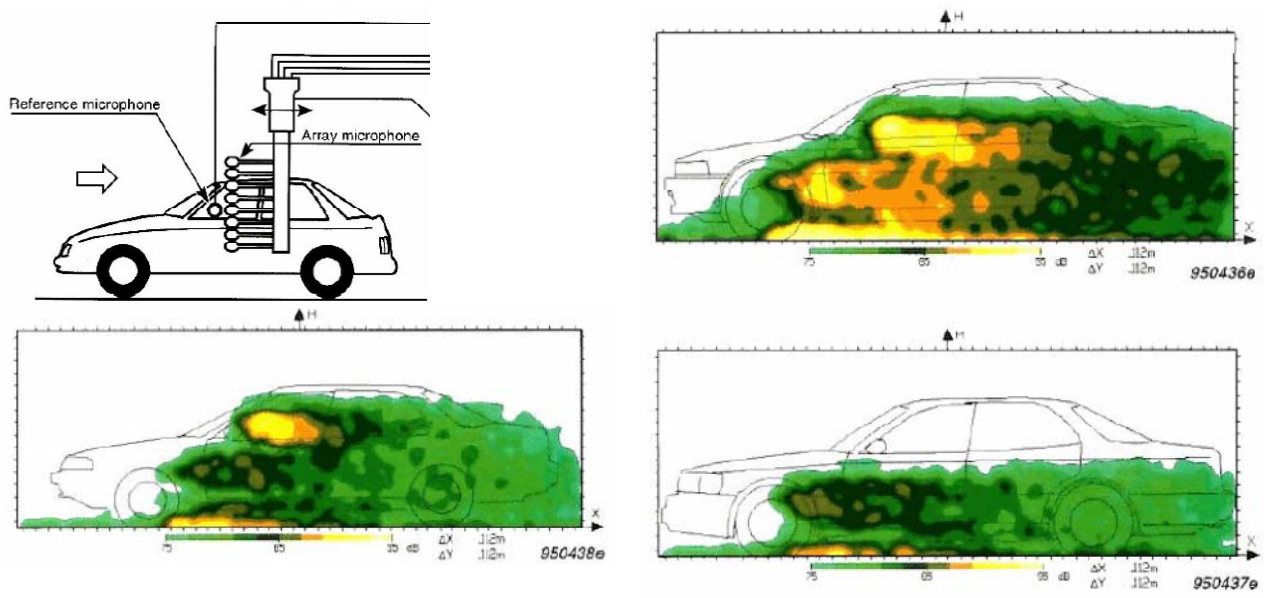

Figure 5: (top left) Holographic set-up for measurement in the Honda low-noise wind-tunnel; (right and bottom left) Outside sound pressure distribution on the side surface of three different cars at a windspeed of 100 km/h. Frequency range is 194 Hz to 792 Hz A-weighted. From[16].

An important practical limitation of AH and NAH resides in the spatial DFT processing. A regular microphone array is needed to obtain a regular spatial sampling of the acoustic field. The spatial spacing between two adjacent microphones depends on the frequency range in study but amounts often to a few centimeters. In the meantime the array is expected to cover the whole source region to minimize the spatial aliasing. This can results in a very large and often prohibitive number of microphones. This situation can be

partly avoided using sequential measurements and reference microphones. However this synchronization technique introduces data loss as soon as the number of incoherent sources is large. Another important drawback is that regular microphone arrangement is the worst array choice for many sound localization techniques such as beamforming. In beamforming irregular arrangements [10] are sought to avoid information redundancy and sidelobe constructive interference. This assertion put NAH apart from other methods because they require a special microphone array. Another drawback of the DFT processing is the spatial windowing effects.

3.1.3 Holography for non-regular arrays: SONAH

A major advance in the field occurred in 2001. To overcome the limitations of the DFT process, Hald [18] proposed a slightly different approach called the Statistically Optimal Near-Field Acoustical Holography (SONAH). In this method the vector $\boldsymbol{p}$ representing the measurement is not anymore constituted of spatial Fourier components but of the complex time-harmonic sound pressure measured at a set of measurement positions. Thus dimension m is now the number of microphones instead of the number of plane wave components chosen to describe the acoustic field. On the contrary $\boldsymbol{q}$ representing the sound field closed to the source is the same than in the NAH method and is filled with wavenumber components. Dimension n is the number of Fourier components used to describe the source sound field; it includes some evanescent plane waves.

The huge advantage of proceeding this way is that planar arrays of arbitrary arrangement can now be used for holography as well as other techniques. This allows to use a complementary approach with the SONAH technique in the lower frequency range for instance (convenient for its advantageous spatial resolution) and beamforming based techniques in the higher frequency range (convenient for their stability).

The price to pay is that the transfer matrix $\boldsymbol{G}$ is now full instead of diagonal since each wavenumber component has a non-zero contribution to the complex pressure in $\boldsymbol{p}$. The analytical expression to fill matrix $\boldsymbol{G}$ is thus similar to eq. (18) except that z_s now depends on the microphone index i and the axial wave number the k_z is depends on the considered column of $\boldsymbol{G}$

$$\boldsymbol{G}_{ij} = e^{\imath k_z^{(j)}(z_h^{(i)} - z_s)} \tag{20}$$

The inversion is thus more time consuming but can be handled using tools presented in section 2.2. A Tikhonov regularization technique can also be used to find a more stable approximate solution.

3.2 Acoustical holography on alternative wave basis

In their original form, holography techniques are based on plane wave decomposition of the sound field. It is perfectly possible to decompose the field on other wave basis such as cylindrical waves [19] or spherical harmonics [20] depending on the set-up geometry. The only requirement is to use a complete basis for the description of the pressure field generated by a source and measured by the array. Each elementary wave is expected to form a solution of the wave equation in the chosen coordinate system.

3.2.1 Cylindrical holography

A variation of the NAH method has been used on an open jet experiment [21]. The cylindrical symmetry of the experiment suggests to use cylindrical wave instead of plane waves in matrix $\boldsymbol{G}$. This gives rise to Cylindrical Near-field Acoustical Holography. It is used for visualizing the sound radiation from an open jet in order to identify the source strength distribution and the radiation patterns (Figure 6). The ability of the cylindrical NAH to quantify noise source in three-dimension and to determine the far field radiation from such a model is demonstrated.

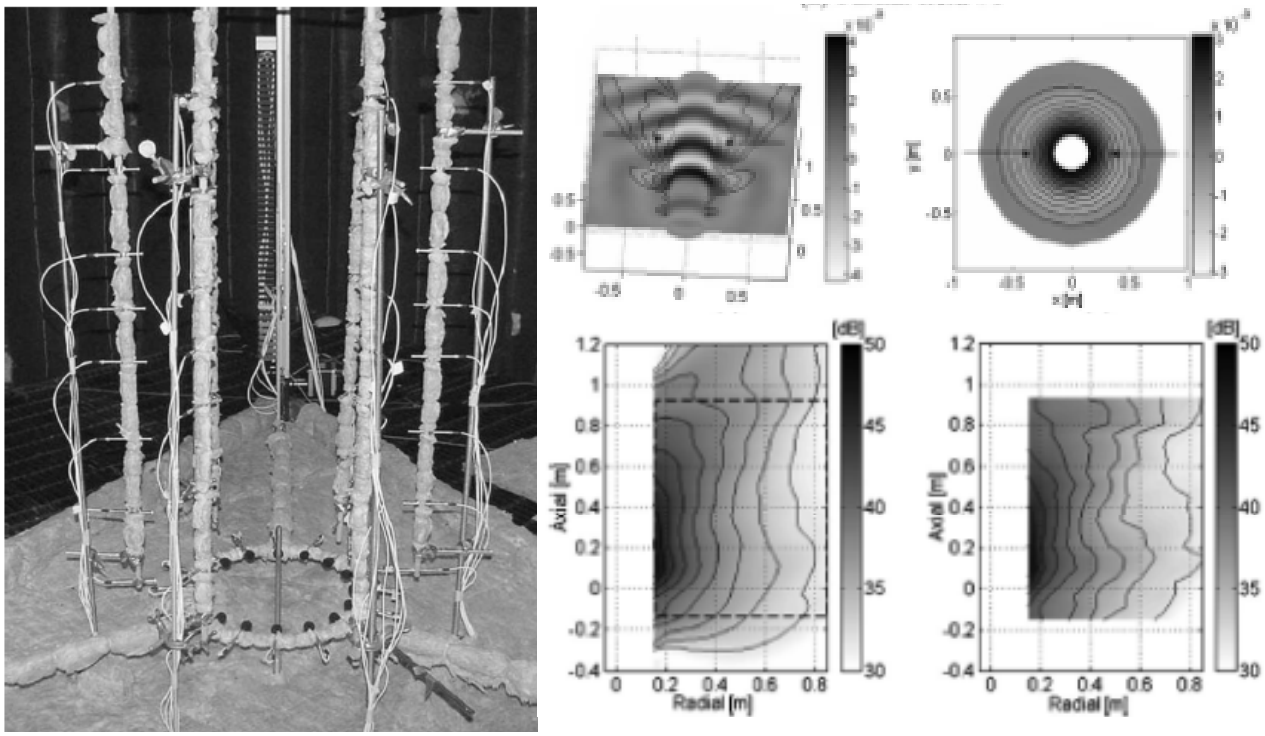

Figure 6: (left) Holographic set-up for measurement (six linear arrays and a circular array); (top right) 3D sound pressure distribution of the first partial field (real part); (bottom middle and right) sound field reconstructed by NAH and measured at 1kHz. From ref [21].

3.2.2 Spherical holography

In situations where the directivity of a specific source is to be investigated, a spherical array can be used such that the source is fully encompassed. This geometry suggests to decompose the pressure field onto the basis of spherical harmonics. These functions are orthonormal to each other and are centered on a specific point of the 3D space, which is often the center of the source of interest. The unknown $\boldsymbol{q}$ vector is then filled with spherical harmonic complex amplitudes, to be determined from the measurement on a sphere of the array radius. A clear and complete description of the spherical near-field acoustic holography method is given in the book of Williams [20]. This method is powerful since it provides a continuous description of the directivity of a single source based on discrete measurements. Moreover an extrapolation of the sound pressure level to the far field can be undertaken in a proper way.

A variation of this method has been developed by [22] with the Field Separation Method. The specificity is that a double microphone layer is used in order to denoise the measurement from external sources in a similar approach than the intensimetry technique.

Another similar technique is the Helmholtz Equation Least Squares (HELS) [23] which uses a single layer of microphones to estimate the velocity field of a vibrating plate. The number of spherical harmonics to be included in $\boldsymbol{G}$ has to be chosen with care and the authors propose an optimization procedure of this parameter, together with a regularization scheme to the inverse problem.

As an industrial example, the FSM has used on the Environmental Control System of a business jet aircraft on ground with a double-layer quarter-sphere array[24].

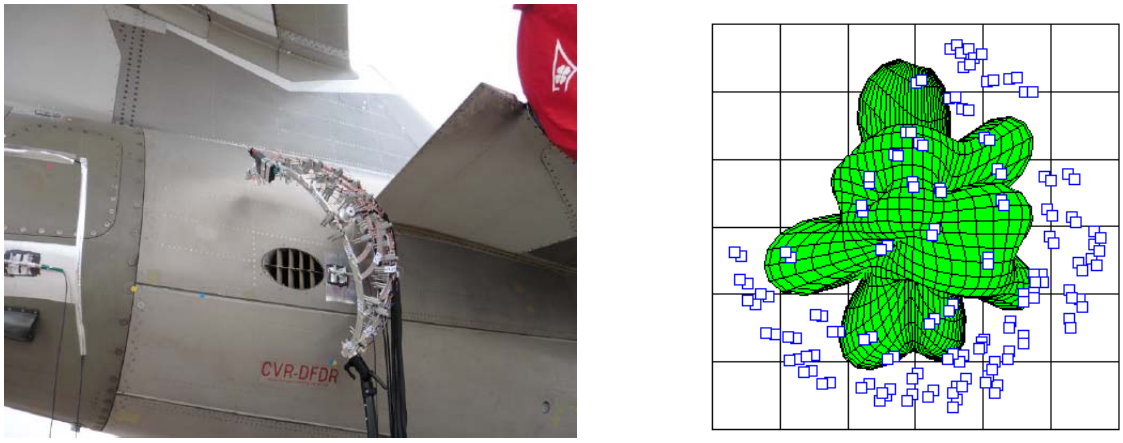

Figure 7: (Left): photograph of array used for the FSM method on the ECS system of a business jet aircraft [24], (right) Computed directivity on tonal noise around 1kHz

3.2.3 Holography for arbitrary wave functions

Plane wave, cylindrical and spherical near-field holography methods are limited in their original formulation to the reconstruction of fields defined by coordinates with separable geometries. A large industrial demand made it possible to generalize the method to any geometry. With the advent of numerical methods and the development of integral methods, inverse methods based on boundary element solver have emerged [25-27], such as iBEM (for Inverse Boundary Element Method). The basic idea is to use a numerical software to fill the transfer matrix $\boldsymbol{G}$. The integral Kirchhoff-Helmholtz equation allows to express the relation between the pressure field measured at a point of the space and the wall pressure or the normal velocity at the wall of the object to be characterized. Two different least-square problems are formulated: the unknown vector $\boldsymbol{q}$ either represent vibrating surface velocity or pressure monopole amplitudes placed on the studied surface. In both cases the integral equation is solved by the Boundary Element Method (BEM). Once the propagation model is known, two distinct inverse problems are successively solved in order to reconstruct the wall pressure and the normal velocity at the wall.

These methods apply both to internal [28] and external [29] acoustic radiation problems. The first publication on the subject dates from the late 1980s [25]. The advantage of this method lies in its geometric flexibility: no constraint on the geometry of the array or object to be characterized is imposed. Nevertheless, it has been shown that the obtained results depend very much on the choice of microphone position [30]. Iterative methods to optimize the positioning of microphones have been developed to ensure independence of the components of the transfer functions. Indeed, the conditioning of the matrix $\boldsymbol{G}$ can be improved by decreasing the degree of dependence between the elements of the model [31]. This method is called "Effective Independance" ("Efi") [28, 30, 32]. For a given frequency range, it makes it possible to determine from among a large number of microphone positions the combination of microphones which ensures an independence of the main components of the transfer matrix.

The iBEM method has two major drawbacks. The first is the computational cost because a BEM solver is required. Indeed, the integral formulation requires a discretization of the object of interest sufficiently fine to respect the rule of 6 nodes per wavelength. The second disadvantage is the non-uniqueness of the solution computed by BEM method [33]. This problem, well known to the numerical experts, is linked to the calculation of irregular resonance frequencies (also called characteristic frequencies) of digital origin which correspond to the internal eigen frequencies of the geometrically isolated elements of the acoustic model.

3.3 Inverse methods based on point sources

Another intuitive development of inverse techniques to sound source location is to use point source models (free field Green functions) in the $\boldsymbol{G}$ matrix instead of a wave description basis. Some techniques belonging to this family are presented in this section: the Inverse Equivalent Source Method, the Generalized Inverse Beamforming and the Bayesian Inference.

3.3.1 Inverse Equivalent Source Method (iESM)

In this method [34], $\boldsymbol{p}$ is one of the principal components (PC, also called eigenmode in the GIB technique) of the cross-spectral matrix (CSM): the eigenvalue decomposition is applied to the CSM $\boldsymbol{C}$ with $\boldsymbol{C} = \boldsymbol{N}\boldsymbol{D}\boldsymbol{N}^*$, $\boldsymbol{N}$ being a unitary matrix and $\boldsymbol{D}$ the diagonal matrix of ordered eigenvalues. A principal component of $\boldsymbol{C}$ is $\boldsymbol{p}_i = \sqrt{\boldsymbol{D}_{\boldsymbol{ii}}}\boldsymbol{N}_{:i}$. Each PC is expected to represent a group of coherent sources. The transfer matrix $\boldsymbol{G}$ is filled with 3D free field Green function (eq. 0.1). In a first approach, the pseudo-inverse tool is used to solve the problem with the addition of a Tikhonov regularization. Two important drawbacks can then be exhibited:

1. The equivalent sources which are close to the array need less energy to generate the same pressure level at the array position than equivalent sources placed farther away. The close sources are favored in the minimization process and are attributed a high amplitude. Localization and quantification problems then arise quickly in configurations where the source domain is large compared to the array size,

2. In simulations, the source power is largely underestimated if it is derived from computed source map $\tilde{\boldsymbol{q}}$, as compared to the injected source power. The reason is that an identified source is represented by a spot of coherent monopoles. Due to the energy minimization principle, phases of the monopoles are such that interference effects produce a directive pattern toward the array. In other words the radiated energy is minimized in regions where no measurement has be carried out. Even if rather intuitive this behaviour leads to underestimated results when addressing monopole sources.

To get rid of these undesirable effects, some modifications have been added to the method. Concerning point 1, a weighting is applied to the columns of matrix $\boldsymbol{G}$ in order to normalize the columns which is the inverse of the distance r_i between each equivalent source and the center of the array. The weighting matrix is then a diagonal matrix noted $\boldsymbol{W}^{(0)}$ with $\boldsymbol{W}_{ii}^{(0)} = 1/r_i$. The problem to be solved is now $\text{minimize}: \|\boldsymbol{p} - \boldsymbol{G}\boldsymbol{q}\|_2^2 + \lambda^2\left\|\boldsymbol{W}^{(0)}\boldsymbol{q}\right\|_2^2$ which is also (eq. 13) using a diagonal weighting matrix $\boldsymbol{C} = \boldsymbol{W}^{(0)}$. The solution is given using a slightly modified form of the pseudo-inverse. To address point 2, it is desired to force the sparsity of the result i.e. to try to limit the interference effect by improving the spatial resolution of the method. Such approach is possible using an iterative procedure. The inverse problem is successively solved using a diagonal weighting matrix $\boldsymbol{W}^{(n)}$ depending on the equivalent source distribution estimated at a previous step $(n-1)$: $\boldsymbol{W}_{ii}^{(n)} = 1/\left|\tilde{q}_i^{(n-1)}\right|$. This weighting of the transfer matrix by the estimated amplitudes of equivalent sources of the previous iteration enhances the sparsity of the source distribution because only equivalent sources of high amplitudes remain in the end of the algorithm. It is the key principle of the Iteratively Reweighted Least Square algorithm to compute sparse reconstruction.

The choice of the regularization parameter in Eq. (13) is a crucial step in order to achieve a good estimate of the reconstructed field. A recent method is derived from the Bayesian framework [35] and is extensively evaluated in [34] by means of numerical and experimental validations. The interest of using the Bayesian regularization criterion in acoustic inverse problems is demonstrated, mostly because thanks to its robustness. iESM being very similar to GIB, a numerical comparison of the two methods is done in [36]. An experimental comparison of this method is provided in **Figure 8: Qualitative comparison of a subset of the NASA 2 case (AIAA Benchmark). Results shown are for the 12.5 kHz one-third octave band. DR means**

diagonal removal. Figure 8 and Figure 9 in the frame of the AIAA array methods benchmark [45]. The legend 'Bayes' actually stands for the iESM technique using a bayesian regularization. NNLS and Bayes source map (Fig. 3) from the University of Lyon contains exactly one source on every slat track and one source on the flap side edge.

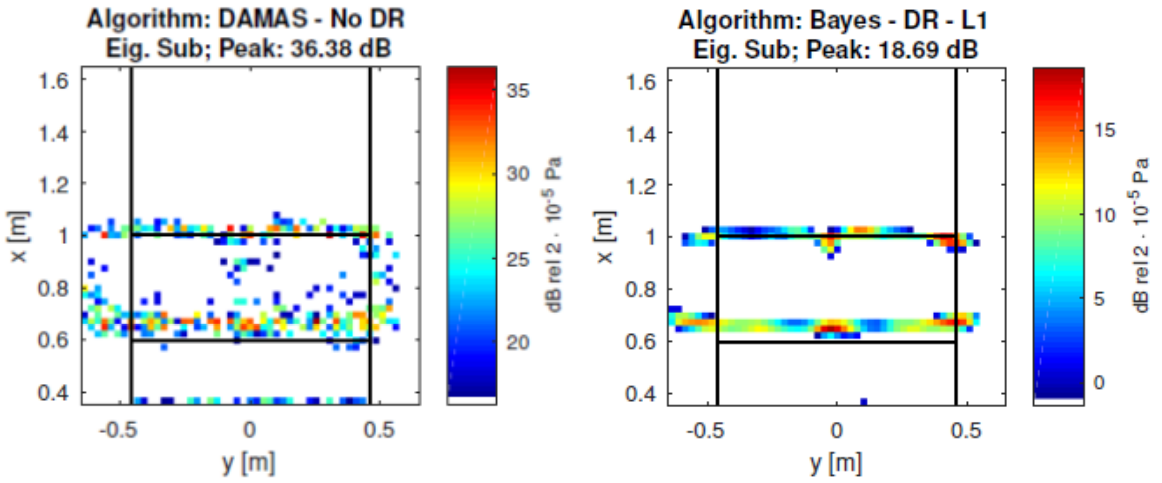

Figure 8: Qualitative comparison of a subset of the NASA 2 case (AIAA Benchmark). Results shown are for the 12.5 kHz one-third octave band. DR means diagonal removal.

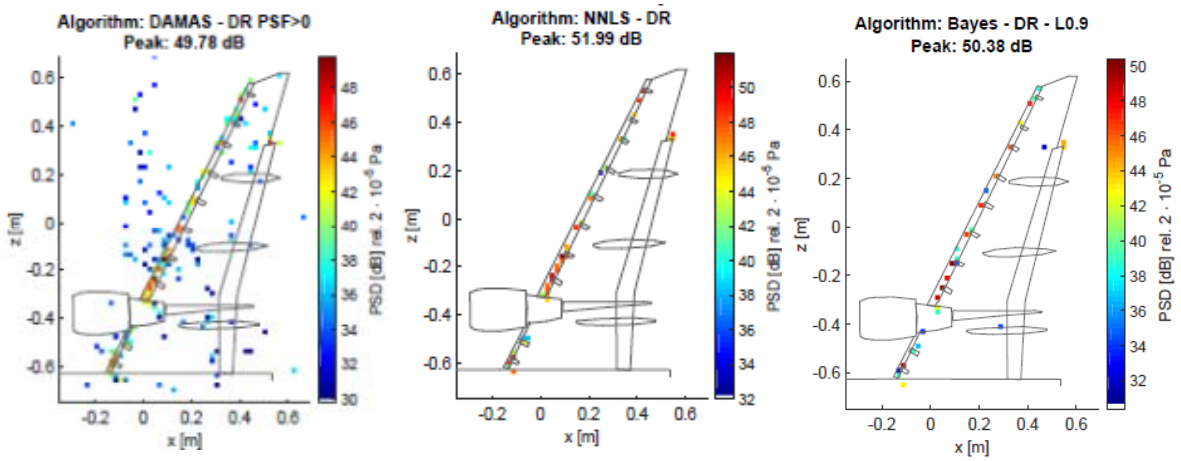

Figure 9: Power spectral density source maps of the Do728 semispan model at the narrowband frequency 8496 Hz with a dynamic range of 20 dB for DAMAS (DLR) and NNLS. PSF>0 means that the point spread function was forced to be nonnegative.

3.3.2 Generalized Inverse Beamforming (GIB)

Ten years ago Suzuki introduced the Generalized Inverse Beamforming (GIB) [37, 38]. The proposed improvements from the classical inverse problem are twofold:

- the unknown vector $\boldsymbol{q}$ is twice the size of the usual monopole source vector: here the upper half describes monopole sources while the lower half part describes dipoles (located at the same place than monopoles). This is rendered by the propagation description in the columns of matrix $\boldsymbol{G}$. This

description allows to draw simultaneous maps of monopoles and dipoles. The least-square process attributes energy either to monopoles or dipoles, depending on the fit with the measurement.

- the source identification problem is written as minimization of an L_p (instead of L_2) norm cost function. While L_2 regularization tends to provide smooth and blur acoustic source maps in terms of localization, the L_p penalization factor proposed by Suzuki (with $0 \leq p \leq 1$) tends to recover the compactness of reconstructed sources. An example given by Suzuki is clarifying this point. Suppose the actual source is a unique monopole of unit amplitude. If a least-square cost function is used to identify this source, it is beneficial to split it in two source of amplitude 0.5. This is because the L_2 norm of the splitted situation $\sum|\tilde{q}_i|^2 = (0.5)^2 + (0.5)^2 = 0.5$ is lower than the L_2 norm of the unique monopole situation$\sum|\tilde{q}_i|^2 = (1)^2 = 1$. This phenomenon does not occur for instance if a L_1 norm is used. Here choice is made to enhance the sparsity of the target solution, i.e. it minimizes the number of equivalent sources with non-zero amplitude, rather than to minimize the total energy of the source map. Finally the L_p-minimization problem is formulated as:

$$\boldsymbol{minimize}: \ \|\boldsymbol{p} - \boldsymbol{G}\boldsymbol{q}\|_2^2 + \lambda^2\|\boldsymbol{q}\|_p^p \tag{21}$$

To solve this L_p-norm inverse problem, an IRLS algorithm is used (Iteratively Reweighted Least Squares) [38]. It consists in computing the least square solution and introducing a diagonal weighting matrix $\boldsymbol{W}^{(n)}$at each iteration n. It is linked to the equivalent source amplitudes which were estimated at the previous iteration $\boldsymbol{W}_{ii}^{(n-1)} = \left|\tilde{\boldsymbol{q}}_i^{(n-1)}\right|^{2-p}$:

$$\tilde{\boldsymbol{q}}^{(n)} = \boldsymbol{W}^{(n-1)}\boldsymbol{G}^*\left(\boldsymbol{G}\boldsymbol{W}^{(n-1)}\boldsymbol{G}^* + \lambda^2\boldsymbol{I}\right)^{-1}\boldsymbol{p}$$

In Suzuki's version of GIB, the regularization parameter λ is determined by a diagonal loading technique similarly to the methodologies employed in Capon algorithms.

Many experimental results have confirmed its applicability to aeroacoustic source mapping (laboratory experiments [38], jet noise [39], jet-flap interaction noise [7]). Figure 7 shows results of a jet –flap interaction study obtained by Suzuki [40] with different methods. It is concluded that conventional beamforming cannot distinguish multipoles, CLEAN-SC works reasonably, and GIB identifies flap dipoles with high resolution.

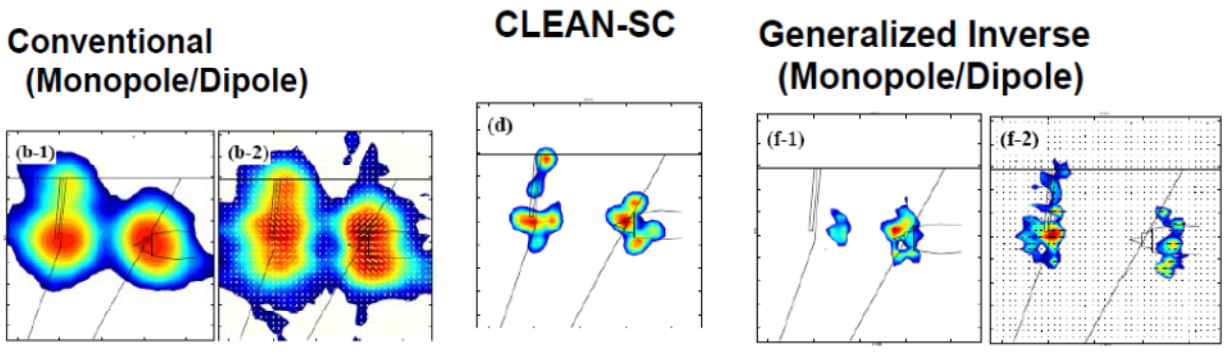

Figure 10: Flap interaction study obtained by Suzuki [40] with different methods; (left) conventional beamforming (monopole/dipole model); (center) CLEAN-SC method (monopole model); (right) GIB method (monopole/dipole model). Approach condition at 12232 Hz.

3.3.3 Bayesian Inference (BI)

As it can be seen throughout this document, information on the physical geometry leads the choice of the method to be used: NAH is a good choice for small planar geometries, Cylindrical NAH is excellent in free jet configurations, FSM in circular configurations etc… A strong aspect of the Bayesian approach is that it is able to automatically tune the optimal decomposition basis of the acoustic field, depending on the geometry and the priori knowledge on the source. Plane waves, cylindrical wave, spherical harmonics are just specific cases. Assuming that a decomposition basis is available, the Bayesian Inference (BI) technique expresses the inverse problem in the standard form

$$\boldsymbol{y} = \widehat{\boldsymbol{S}}\boldsymbol{c} \tag{22}$$

Where $\boldsymbol{y}$ is the coordinate vector in this basis of the measurement vector $\boldsymbol{p}$, $\boldsymbol{c}$ is the vector of source coefficient expressed in this basis and $\widehat{\boldsymbol{S}}$ is the propagation operator matrix which turns out to be a diagonal matrix. This is not a coincidence, since the "optimal basis" in the Bayesian sense has been specifically designed to have this property [35]. The solution is computed with a Tikhonov regularization. The regularization parameter is chosen using a Bayesian technique already encountered (but not detailed) in section 3.3.1 in the iESM technique. A first special feature of the BI method is thus the tuning of the optimal basis; it is briefly introduced at the end of this section. In situation where a regular plane array is placed in nearfield of a plate, the optimal basis calculated by Bayesian approach is the plane wave basis. The method can also be used to characterize objects with complex 3D shape [44].

Another feature of the BI is the use of an inverse technique in a statistical context. In acoustics, energetic quantities are modelled by probability density functions (pdf). A realization of the random variable could be a Fourier coefficient of a FFT snapshot (at the discrete frequency under study). Experimental errors are modelled by a zero-mean Gaussian pdf [42], as a consequence of the Central Limit Theorem. Noise correlation between microphones can be modelled by a covariance matrix $\boldsymbol{\Omega}_b$, often chosen diagonal. The variance of the pdf is noted β^2 and it represents the energy of the noise. Its value is unknown. The Bayesian technique is also interesting because it presents a rigorous framework to add prior information which is of great help in the sound source localization process [41]. For instance the pdf of unknown complex amplitudes $\mathbf{q}$ placed at each node included in the source grid is usually modelled using a zero-mean Gaussian law: before measurements, the probability of having negative and positive amplitude is the same for all the nodes. Modelling the pdf of the sources (also called prior pdf) with a Gaussian law is a first prior information: the energy of the source is finite and it is modelled by the unknown variance of the pdf, noted α^2. One could also add a spatial prior information to attribute greater importance on areas containing potential sound sources, or use the information about the spatial coherence properties of the source. The prior on the source covariance is represented by a noise source covariance matrix $\boldsymbol{\Omega}_q$ of size $[n, n]$, which is often chosen diagonal.

To compute the optimal basis, a SVD is operated on the propagation operator whitened by the two covariance matrices: $\boldsymbol{\Omega}_b{}^{-1/2}\boldsymbol{G}\boldsymbol{\Omega}_q{}^{1/2} = \widehat{\boldsymbol{U}}\widehat{\boldsymbol{S}}\widehat{\boldsymbol{V}}^*$**.** Then the transfer matrix $\boldsymbol{\Phi}$ from the source physical space to the optimal space is computed using

$$\boldsymbol{\Phi} = \boldsymbol{\Omega}_q{}^{1/2}\,\boldsymbol{G}^*\widehat{\boldsymbol{S}}^{-1}\boldsymbol{\Omega}_b{}^{-1/2}\widehat{\boldsymbol{U}} \tag{23}$$

The solution $\tilde{\boldsymbol{q}}$ is computed from the estimate $\tilde{\boldsymbol{c}}$ in this optimal space by $\tilde{\boldsymbol{q}} = \boldsymbol{\Phi}\tilde{\boldsymbol{c}}$. Similarly, the coordinates of the measurement vector in this reference frame is computed using

$$\boldsymbol{y} = \widehat{\boldsymbol{U}}^*\boldsymbol{\Omega}_b{}^{-1/2}\boldsymbol{p} \tag{24}$$

The most probable solution $\tilde{\boldsymbol{q}}$ is the source distribution which provides the best compromise between the fidelity to the noisy measured data $\boldsymbol{p}$ and the prior information $\boldsymbol{\Omega}_q$. This compromise is given by the Bayes rule which expresses the posterior source distribution by the product of the pdf of the measured data and

the prior distribution. The first term is a Gaussian law and it is called the likelihood distribution. Its mean is equal to the amplitude of the measured amplitude on each microphone and its variance is equal to the energy of the noise β^2. The second term has been examined before. The product of these two pdf gives another Gaussian law, as illustrated in Figure 11. The most probable value is given by the maximum of this posterior pdf called MAP (maximum a posteriori). It has been proven that the maximum of this pdf is equivalent to the Tikhonov form solution.

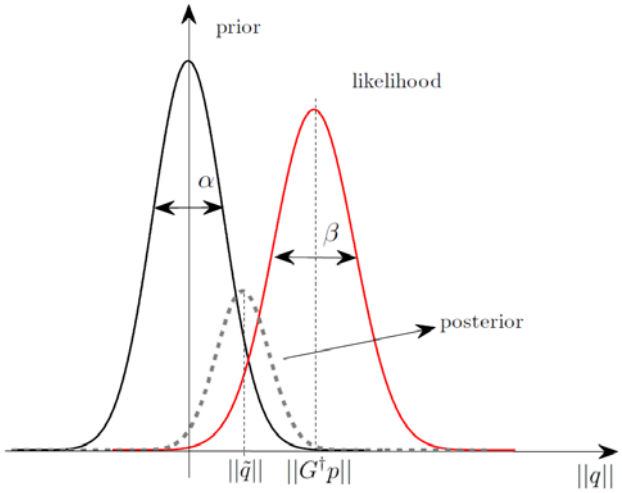

Figure 11 : Schematic 1D representation of the Bayesian framework simplified from the reference [43]. The figure illustrates the Bayes rule which expresses the posterior distribution (dotted line) as the product of the likelihood distribution (in red line) and the prior distribution (in black line).

In the figure, we can observe that the maximum value of the posterior pdf is highly dependent on the values of the two standard deviation α^2 and β^2. It turns out that the ratio of these two quantities definite the regularization parameter: $\eta^2=\alpha^2/\beta^2$. If the measured data are informative and noise-free, η^2 is high and the MAP follows the measurement. Contrary, if η^2 is low, the solution is driven by the prior information. The optimal estimation of the regularization parameter is also given by applying the Bayes rule [43]. Moreover, if a uniform prior distribution is assumed (no prior about the finite energy of the sources), the solution depends uniquely on the likelihood and the MAP estimator is equal to the pseudo-inverse of the propagator times the measurement.

4.0 CONCLUSION

In this document basic tools of least-square minimization problems are presented, as they are used in sound source identification inverse techniques. The pseudo-inverse operator is introduced as the exact solution of the naïve problem having the minimum norm. Stability problems and the importance of the transfer matrix condition number have been discussed. Some regularization methods have been introduced such that the least-square Tikhonov regularization. Most famous methods of the regularization parameter selection have been briefly presented. Other advance regularization such as sparse regularization have also been mentioned.

The second part of the document is dedicated to application methods. Planar methods are presented: acoustic holography, nearfield acoustic holography, statically optimized nearfield acoustic holography. Holography in cylindrical and spherical coordinate systems are also presented, as well as holography for arbitrary wave functions. In a final part, inverse method based on point source transfer functions are introduced, namely the iESM method, the Generalized inverse beamforming and the Bayesian Inference.

The common basis of all these methods has been emphasized, together with the specific development and innovation in each of them. It is hoped that the reader would find in this document a clear grasp of the rich domain of inverse techniques applied to sound source localization. Given references are also proposed as

valuable and didactical entry points for who is willing to get into more details.

REFERENCES

[1] *Modal Testing: Theory and Practice*. **D. J. Ewins**. Mechanical Engineering Research Studies: Engineering Dynamics Series, 1985.

[2] *Estimation of acoustic source strength by inverse methods: Part I, conditioning of the inverse problem*. **P. A Nelson, S.-H. Yoon**. Journal of sound and vibration, volume 233, issue 4, 2000.

[3] *Estimation of acoustic source strength by inverse methods: Part II, experimental investigation of methods for choosing regularization parameters*. **P. A Nelson, S.-H. Yoon**. Journal of sound and vibration, volume 233, issue 4, 2000.

[4] *A unified formalism for acoustic imaging techniques: illustrations in the frame of a didactic numerical benchmark.* **Leclère, Quentin, et al.** Berlin Beamforming Conference 2016 : s.n., 2016.

[5] *Generalized Inverses of Linear Transformations*. **S. L. Campbell and C. D. Meyer Jr**. Dover Publications 1991.

[6] *Sparsity constrained deconvolution approaches for acoustic source mapping*. **Tarik Yardibi, Jian Li, Petre Stoica, and Louis N. Cattafesta III.** The Journal of the Acoustical Society of America 123, 2008.

[7] *L1 generalized inverse beam-forming algorithm resolving coherent/incoherent, distributed and multipole sources*. **T. Suzuk**i. J. Sound Vib., 330, 5835–5851, 2011.

[8] *Near-field acoustic holography using sparse regularization and compressive sampling principles*. **G. Chardon, L. Daudet, A. Peillot, F.Ollivier, N. Bertin and R. Gribonval**. The Journal of the Acoustical Society of America 132, 2012.

[9] *A robust super-resolution approach with sparsity constraint in acoustic imaging*. **N. Chu, J. Picheral, A. Mohammad-Djafari and N. Gac**. Applied Acoustics 76:197–208, February 2014

[10] *Une approche bayésienne de la parcimonie pour l'identification de sources acoustiques*. **Q. Leclere, A. Pereira, and J. Antoni.** In Proceedings of CFA 2014, (Poitiers, France), 2014.

[11] *Holographic imaging without the wavelength resolution limit*. **E.G. Williams and JD Maynard**. Physical review letters, 45(7) :554–557, 1980.

[12] *Sound source reconstructions using a microphone array*. **E.G. Williams, JD Maynard, and E. Skudrzyk**. The Journal of the Acoustical Society of America, 68 :340, 1980.

[13] *Nearfield acoustic holography : I. theory of generalized holography and the development of nah*. **J.D. Maynard, E.G. Williams, and Y. Lee**. The Journal of the Acoustical Society of America, 78 :1395, 1985.

[14] *Nearfield acoustic holography (nah) ii. Holographic reconstruction algorithms and computer implementation*. **W.A. Veronesi and J.D. Maynard.** The Journal of the Acoustical Society of America, 81 :1307, 1987.

[15] *STSF - a unique technique for scan-based Near-field Acoustic Holography without restrictions on coherence*. **J. Hald**. Technical Review, Brüel & Kjaer, 1989.

[16] *Sound Fields (STSF) Techniques in the Automotive Industry*. **J. Hald**. Technical Review, Brüel &

Kjær, 1995.

[17] *Aeroacoustic measurements*. **T. J. Mueller**. Springer Science & Business Media, 2002.

[18] *Time domain acoustical holography and its applications*. **J. Hald**. Sound and Vibration, 35(2) :16–25, February 2001.

[19] *Source visualization by using statistically optimized near-field acoustical holography in cylindrical coordinates*. **Y. T. Cho, J. S. Bolton, and J. Hald**. The Journal of the Acoustical Society of America, 118(4) :2355–2364, 2005.

[20] *Fourier Acoustics: Sound Radiation and Nearfield Acoustical Holography*. **E. G. Williams**. Academic Press, 1999.

[21] *Source characterization of a subsonic jet by using near-field acoustical holography*. **L. Moohyung and J. Stuart Bolton**. The Journal of the Acoustical Society of America, 121(2), 2007.

[22] *Evaluation of a separation method for source identification in small spaces*. **Y. Braikia, M. Melon, C. Langrenne, E. Bavu, and A. Garcia**. J. Acoust. Soc. Am. 134, n° 1, 2013.

[23] *Helmholtz equation–least-squares method for reconstructing the acoustic pressure field*. **Z. Wang, and S. Wu**. J. Acoust. Soc. Am. 104, n° 4, 1997.

[24] *Directivity measurement of an ECS outlet on a business jet aircraft on ground*. **A. Finez, and S. Barré**. AIAA/CEAS 2016-2766. Lyon, 2016.

[25] *Digital holographic reconstruction of sources with arbitrarily shaped surfaces*. **W.A. Veronesi and J.D. Maynard**. The Journal of the Acoustical Society of America, 85 :588, 1989.

[26] *Sound source reconstruction using inverse boundary element calculations*. **A. Schuhmacher, J. Hald, K.B. Rasmussen, and P.C. Hansen**. The Journal of the Acoustical Society of America, 113 :114, 2003.

[27] *Implicit methods of solution to integral formulations in boundary element method based nearfield acoustic holography*. **N. Valdivia and E.G. Williams**. The Journal of the Acoustical Society of America, 116 :1559, 2004.

[28] *On the reconstruction of the vibro-acoustic field over the surface enclosing an interior space using the boundary element method*. **B.-K. Kim and J.-G. Ih**. The Journal of the Acoustical Society of America, 100 :3003, 1996.

[29] *Application of bem (boundary element method)-based acoustic holography to radiation analysis of sound sources with arbitrarily shaped geometries*. **M.-R. Bai**. The Journal of the Acoustical Society of America, 92 :533, 1992.

[30] *Sensor placement for on-orbit modal identification and correlation of large space structures*. **D. C. Kammer**. Journal of Guidance, Control, and Dynamics, 14(2) :251–259, 1991.

[31] *Etude et développement de la mesure indirecte d'efforts - Application à l'identification des sources internes d'un moteur Diesel*. **Q. Leclère**. PhD thesis, INSA de Lyon, 2003.

[32] *On the holographic reconstruction of vibroacoustic fields using equivalent sources and inverse*

boundary element method. **I.Y. Jeon and J.G. Ih**. The Journal of the Acoustical Society of America, 118 :3473, 2005.

[33] *Improved integral formulation for acoustic radiation problems*. **H. A. Schenck**. The Journal of the Acoustical Society of America, 44(1) :41–58, 1968.

[34] *Acoustic imaging in closed spaces*. **A. Pereira**. PhD thesis, INSA de Lyon, 2013.

[35] *A bayesian approach to sound source reconstruction: Optimal basis, regularization, and focusing*. **J.Antoni**. The Journal of the Acoustical Society of America, 131(4), 2873–2890, 2012.

[36] *A theoretical and experimental comparison of the iterative equivalent source method and the generalized inverse beamforming.* **B. Oudompheng, A. Pereira, C. Picard, Q. Leclere, and B. Nicolas**. In Proceedings of the 5th Berlin Beamforming Conference, 19-20 February 2014.

[37] *Generalized Inverse Beam-forming Algorithm Resolving Coherent/Incoherent, Distributed and Multipole Sources*. **T. Suzuki**. AIAA-2008-2954, 2008.

[38] *Generalized inverse beamforming investigation and hybrid estimation*. **P. A. G. Zavala, W. de Roeck, K. Hanssens, J. R. de Franca Arruda, P. Sas, and W. Desmet**. BeBeC-2010-10. Proceedings on CD of the 3rd Berlin Beamforming Conference, 24-25 February, 2010.

[39] *Improved Generalized Inverse Beamforming for Jet Noise*. **R. P. Dougherty**. AIAA-2011-2769, 2011. 17th AIAA/CEAS Aeroacoustics Conference (32nd AIAA Aeroacoustics Conference), Portland, Oregon, June 5-8, 2011.

[40] *L1 generalized inverse beam-forming in applications to aeroacoustic problems*. **T. Suzuki**. 161st Meeting of ASA, Seattle WA, 2011.

[41] *Approche bayésienne pour les problèmes inverses*. **J. Idier**. Traité IC2, Série traitement du signal et de l'image, Hermès, Paris, 2001

[42] *Mathematical Methods of Statistics (PMS-9)*. **H. Cramer**. Princeton university press, 1999.

[43] *Empirical Bayesian regularization of the inverse acoustic problem*. **Q. Leclère, A. Pereira, and J. Antoni**. Applied Acoustics, 2015.

[44] *Approche multidimensionnelle du problème d'identification acoustique inverse*. **T. Le Magueresse**. PhD thesis, INSA de Lyon, 2016.

[45] *A Comparison of Microphone Phased Array Methods Applied to the Study of Airframe Noise in Wind Tunnel Testing*. **C. J. Bahr, W. M. Humphreys Jr., D. Ernst, T. Ahlefeldt, C. Spehr, A. Pereira, Q. Leclère, C. Picard, R. Porteous, D. J. Moreau, J. Fischer and C. J. Doolan**. 23rd AIAA/CEAS Aeroacoustics Conference, Denver, CO, 2017.